Available online at www.sciencedirect.com

ScienceDirect

Ceramics International 40 (2014) 241–248

CERAMICS INTERNATIONAL

www.elsevier.com/locate/ceramint

Characterization and spectral studies of Co^{3+}-doped $Cd_{0.4}Mn_{0.6}Fe_2O_4$ ferrites

M.A. Amer[a,*], T.M. Meaz[a], A.G. Mostafa[b], M. El-Kastawi[c], A.I. Ghoneim[a]

[a]*Physics Department, Faculty of Science, Tanta University, 31527 Tanta, Egypt*
[b]*ME Laboratory, Physics Department, Faculty of Science, Al-Azhar University, Egypt*
[c]*Physics Department, Faculty of Science, Swiz Canal University, Swiz, Egypt*

Received 20 April 2013; received in revised form 5 May 2013; accepted 31 May 2013
Available online 7 June 2013

Abstract

A series of the $Cd_{0.4}Mn_{0.6}Co_xFe_{2-x}O_4$ ferrites, $0 \le x \le 1$, were prepared and studied by using X-ray patterns and Mössbauer and FMR spectra. The lattice parameter, mean ionic radii and hopping and bond lengths and edges are determined and discussed as functions of Co^{3+} content x. The obtained value of oxygen positional parameter was 0.397 for all samples. The recorded FMR and Mössbauer spectra indicated a ferrimagnetic nature of all the samples. The spin–spin relaxation time, the Lande factor (g), line width ΔH and the resonance field are affected by the Co^{3+} additions x. The Mössbauer spectra were analyzed to two sextets attributed to the Fe^{3+} ions at A- and B-sites. The quadrupole and isomer shift values are found to be independent on x, whereas the hyperfine magnetic fields, H_A and H_B, and Mössbauer line widths at the A- and B-sites, respectively, showed dependence on x. Also H_A and H_B were affected by the hopping and bond lengths at these sites.

Keywords: D. Ferrites; Cd–Mn–Co; X-ray; Mössbauer; FMR and magnetic properties

1. Introduction

Ferrites continue to be very attractive materials for technological applications due to their combined properties as magnetic conductors (ferrimagnetic) and electric insulators. Polycrystalline ferrites have applications ranging from simple lifting magnets, microwave frequencies, radio frequencies to the most complex microwave communications to outer space. Many efforts of research have performed in studying the preparation and properties of spinel ferrites [1–10]. Spinel ferrites, by virtue of their structure, can accommodate a variety of cations at different sites enabling a wide variation in electrical and magnetic properties.

Spinel ferrites with cubic crystal structures have interesting structural, physical and magnetic properties. These properties of ferrites strongly depend on the chemical composition, the electronic structure of the magnetic ions, preparation conditions, and the crystal structure of the lattice. The important quantities for technical applications depend also to a great extent on the microstructure of the product [1–10].

The present work is devoted to study the effect of trivalent Co ions substitution for Fe^{3+} ions of spinel ferrites $Cd_{0.4}Mn_{0.6}Co_xFe_{2-x}O_4$, $0 \le x \le 1$, on structural, magnetic and site-ionic properties. The techniques used are X-ray patterns, Mössbauer and ferromagnetic resonance spectra.

2. Experimental

A series of the $Cd_{0.4}Mn_{0.6}Co_xFe_{2-x}O_4$ ferrite samples, x=0.0, 0.125, 0.25, 0.375, 0.5, 0.75 and 1, were prepared by the high temperature solid state reaction method. Molar ratios of the high purity CdO, MnO, Co_2O_3 and Fe_2O_3, were mixed together and milling in agate mortar. The final products were pre-sintered at 1000 °C for 24 h and furnace cooled to room temperature. The samples were ground, pelletized and sintered at 1200 °C for 24 h and cooled slowly to room temperature.

X-ray diffraction patterns were recorded using X-ray diffractometer of the type PRUKER-DX and CuK_α radiation.

*Corresponding author. Tel.: +20 403344352; fax: +20 403350804.
E-mail address: moazamer@hotmail.com (M.A. Amer).

0272-8842/$ - see front matter © 2013 Elsevier Ltd and Techna Group S.r.l. All rights reserved.
http://dx.doi.org/10.1016/j.ceramint.2013.05.130

The lattice parameter a was calculated using the relation; $a=d(h^2+k^2+l^2)^{1/2}$, where d is the interplanar distance obtained by the Bragg's relation; $2d\sin\theta=n\lambda$, where θ is the diffraction angle and λ is the X-ray wavelength (λ=1.5405 Å).

Ferromagnetic resonance (FMR) spectra of the samples were recorded using JSE-Fe 2xG Jeol EPR spectrometer at room temperature. The FMR spectra were recorded as a first derivative of the absorbed spectra.

A constant acceleration computerized Mössbauer spectrometer and 25 mCi ^{57}Fe radioactive sources diffused in rhodium matrix were used and metallic iron was used for calibration. The obtained spectra were analyzed and fitted using a computer program based on Lorenzian line shapes.

3. Results and discussion

3.1. X-ray analysis

Fig. 1 shows the X-ray diffraction patterns of the $Cd_{0.4}Mn_{0.6}Co_xFe_{2-x}O_4$ ferrites. It is shown that the reflection planes (111), (220), (311), (222), (440), (422), (511), (440), (620), (533), (622) and (444) appeared for all the samples, which prove that these samples are single phase of cubic spinel ferrites [11]. The calculated values of the lattice parameter a lie between 8.5005 and 8.5548 Å, which agree with the previous studies [1,5]. The average values of a are plotted against x as seen in Fig. 2. It is seen that a decreases slowly with x, which is attributed to the substitution of Fe^{3+} ions (0.64 Å) by the smaller Co^{3+} ions (0.61 Å).

Fig. 3 displays that X-ray density D_x and bulk density D increase, while the porosity P decreases with x. The increase in D_x and D with x may be attributed to the substitution of the larger atomic weight Co^{3+} (58.93) by Fe^{3+} (55.85). The decrease in porosity with x may be due to the densification of the samples by sintering process. The X-ray patterns indicated that the peak (311) is a little shifted to higher θ values in samples for $x\geq0.5$, which may be ascribed to the increase in packing which is emphasized by the porosity.

The mean ionic radii of the A- and B-sublattices (R_A and R_B) can be calculated for all samples using the cation distribution and the relations [6,7];

$$R_A = 0.4r_{Cd^{2+}} + (0.6-y)r_{Mn^{2+}} + zr_{Co^{3+}} + yr_{Fe^{3+}}$$

$$R_B = yr_{Mn^{2+}} + (x-z)r_{Co^{3+}} + (2-y-x)r_{Fe^{3+}}$$

where r denotes to the ionic radius and y and z to the number of Fe^{3+} and Co^{3+}ions at the A-sites, respectively. The calculated values are given in Table 1. It is obvious that the trend of R_A and R_B decrease with x, which may be due to the substitution process. The oxygen positional parameter u can be determined using the relation [6,7];

$$R_A = a\sqrt{3}(u-0.25)-r_O$$

where r_o is the O^{2-} radius. The obtained value of u was 0.397 for all samples. The tetrahedral bond length $d_{AL}(d^{2-}_{A-O})$ and the octahedral bond length $d_{BL}(d^{2-}_{B-O})$ can be calculated by the relations [6,7];

$$d_{AL} = a\sqrt{3}(u-0.25)$$

$$d_{BL} = a\left(3u^2-\frac{11}{4}u+\frac{43}{64}\right)^{1/2}$$

The tetrahedral edge d_{AE} and the octahedral edge d_{BE} and unshared edge d_{BEU} can be determined using the relations [6,7];

$$d_{AE} = a\sqrt{2}(2u-0.5)$$

$$d_{BE} = a\sqrt{2}(1-2u)$$

$$d_{BEU} = a\left(4u^2-3u+\frac{11}{16}\right)^{1/2}$$

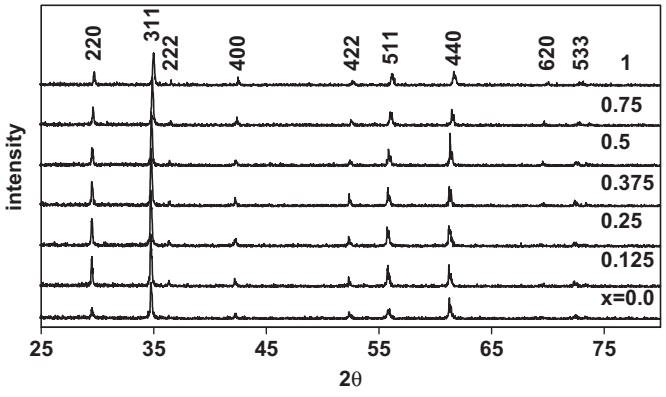

Fig. 1. X-ray diffraction patterns for the system $Cd_{0.4}Mn_{0.6}Co_xFe_{2-x}O_4$.

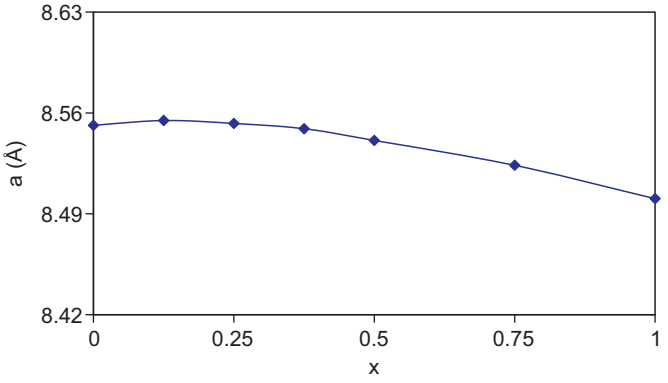

Fig. 2. Dependence of the lattice parameter a on Co^{3+} ion content x.

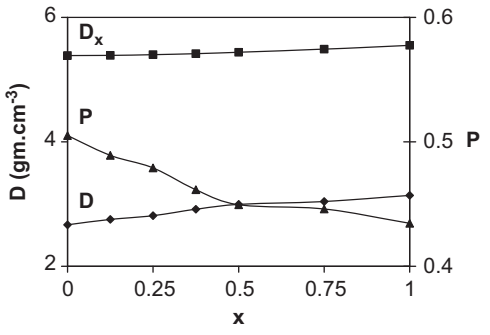

Fig. 3. x dependence of the X-ray density (D_x), bulk density (D) and porosity (P).

Table 1
The obtained lattice parameters, where R_A and R_B are the ionic radii of the A- and B-sites, a the lattice parameter, d_{AL}, d_{BL} the A- and B-site bond lengths, d_{AE} the tetrahedral edge and d_{BE} and d_{BEU} the octahedral shared and unshared edges and L_A, L_B are hopping lengths at A- and B-sites, respectively.

x	R_A (Å)	R_B (Å)	a(Å)	d_{AL} (Å)	d_{BL} (Å)	d_{AE} (Å)	d_{BE} (Å)	d_{BEU} (Å)	L_A (Å)	L_B (Å)
0.0	0.77	1.29	8.55	2.172	1.97	3.547	2.5	3.046	3.703	3.023
0.125	0.77	1.288	8.555	2.17	1.97	3.544	2.5	3.044	3.704	3.025
0.25	0.768	1.286	8.553	2.168	1.97	3.541	2.501	3.043	3.704	3.024
0.375	0.767	1.284	8.55	2.167	1.97	3.539	2.5	3.042	3.702	3.023
0.5	0.766	1.282	8.54	2.166	1.965	3.536	2.494	3.038	3.698	3.02
0.75	0.764	1.276	8.524	2.164	1.963	3.533	2.49	3.034	3.691	3.014
1	0.762	1.27	8.501	2.162	1.955	3.530	2.477	3.026	3.681	3.005

The distance between the magnetic ions Co^{3+} and Fe^{3+} (hopping lengths) can be calculated by the relations $L_A=a_t\sqrt{3/4}$ and $L_B=a_t\sqrt{2/4}$ for A- and B-sublattices [9]. The determined values are listed in Table 1.

Table 1 illustrates that the trends of R_A, R_B, d_{AL}, d_{BL}, d_{AE}, d_{BE}, d_{BEU}, L_A and L_B reflect the same behavior of a and decrease against x. This is assigned to the substitution process and cation distribution. The values of u are higher than the standard values (0.375), which may point to a trigonal distortion of the B-site coordination. It may be due to the oxygen dissociation through the samples during the preparation.

3.2. Ferromagnetic resonance (FMR) spectra

The absorption of microwave power signal in soft ferrites around zero field has been observed and studied early, where it was clearly distinct to ferromagnetic resonance (FMR) [5,12–15]. Fig. 4 shows the resonance spectra of the $Cd_{0.4}Mn_{0.6}Co_xFe_{2-x}O_4$ samples at room temperature. It is shown that the resonance spectra exhibit a single broad signal, a change in their line shape and a shift in resonant field (H_{res}) with increasing Co^{3+} content x. The single broad signal with no sign of saturation indicates that Fe^{3+}, Mn^{2+}, Cd^{2+} and Co^{3+} ions co-exist. All spectra exhibit a symmetric broad resonance signal, but their peak-to-peak line width (ΔH_{pp}) and resonant magnetic field (H_r) are different from each other.

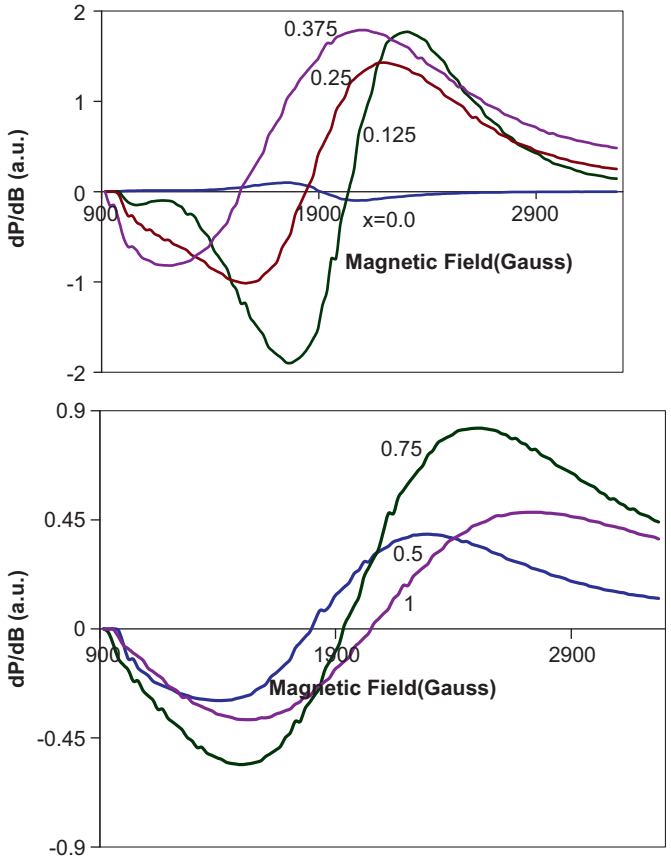

Fig. 4. Resonance spectra of $Cd_{0.4}Mn_{0.6}Co_xFe_{2-x}O_4$ at room temperature.

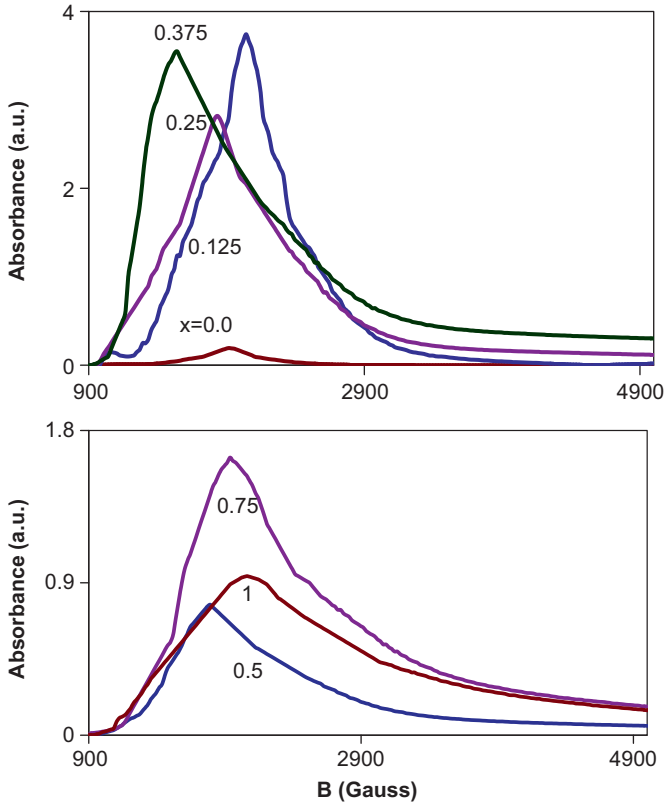

Fig. 5. The absorption power as a function of magnetic field.

For estimation of the line width, resonance field and area under the peak the first derivative spectra were converted into absorption curves as illustrated in Fig. 5. The resonance field (H_r) is defined as the field at which $dP/dH=0$ and is given by [16]:

$$H_r = \frac{\omega}{\gamma}$$

where ω is the excitation frequency and γ is the gyromagnetic factor for free electrons. The variation of H_r and the line width ΔH with x is illustrated in Fig. 6. It is illustrated that the values of H_r decreases to a minimum at $x=0.375$ and increases thereafter, whereas ΔH increases. The variation of H_r may be attributed to the effect of the anisotropy, porosity, inhomogeneous demagnetization, saturation magnetization and internal field on H_r [13]. The increase of the line width ΔH can be explained by the existence of the divalent ions Fe^{2+}, Mn^{2+}, Cd^{2+} and Co^{2+} among octahedral B-sites, which can cause a broadening of line width. Large ΔH means high field absorption and more electric loss.

The Lande' factor (g) equals 2.0023 for an isolated free electron, and has different values in the solid environment. Fig. 7 evidences that the g-value increases versus x to a maximum value at $x=0.375$. It is evidenced that the g-values are slightly higher than that of the free electron value. The variation of g-factor values may be attributed to the variation of porosity.

3.3. Mössbauer spectra

Fig. 8 shows the room temperature Mössbauer spectra of the ferrite system $Cd_{0.4}Mn_{0.6}Co_xFe_{2-x}O_4$. The spectra show a

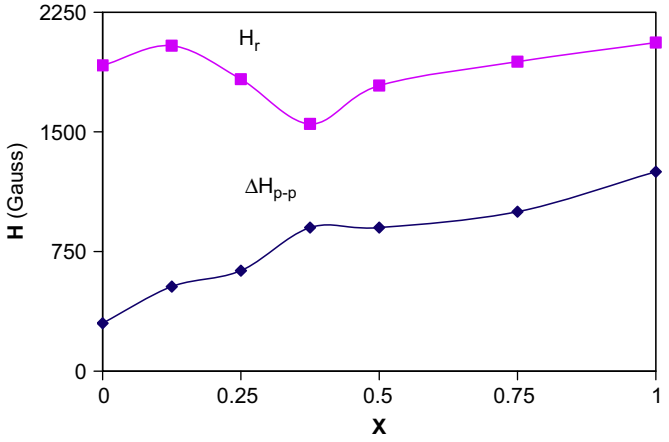

Fig. 6. The resonance field H_r and the line width ΔH as functions of Co^{3+} content x.

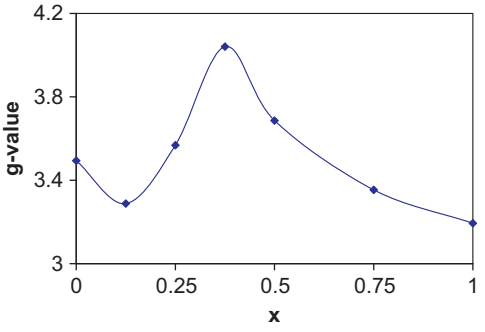

Fig. 7. The relation between g-factor and x.

relaxed magnetic Zeeman pattern for all samples. The relaxation of spectra may be arise from the chemical disorder of cations in the samples i.e. existence of cations of different radii and charges in the sublattices. The spectra have been analyzed to two subspectra, the sharper is ascribed to Fe^{3+} ions among the tetrahedral A-site (A) and the broader to Fe^{3+} ions at the octahedral B-site (B). The broader octahedral subspectrum has been analyzed to its multicomponents B_n ($n=0, 1,\ldots, 5$) for all samples. The obtained results from the fitting are given in Table 2. In most magnetically ordered spinel phases, Neel ordering is determined mainly by the strong anti-ferromagnetic A–B interactions and the contribution of A–A and B–B interactions is weak.

The presence of B-site multi-components should be expected because of the distribution of hyperfine fields at the B-site caused principally by a random distribution of the nonmagnetic Cd^{2+} ions and to less extent by the magnetic Mn^{2+}, Co^{3+} and/or Fe^{3+} ions at the A-site [17]. Therefore, octahedral Fe^{3+} cations have different numbers of Cd^{2+} ions occupying its six nearest neighbors at A-sites. Consequently, the superexchange interaction of each B cation with its six A- nearest neighbor cations depends on the population of Cd^{2+} ions among the six A-cations, which in turn affects the hyperfine field at the Fe nucleus of the B-cation. In addition, the s-electron density at the nucleus of this B-cation is also

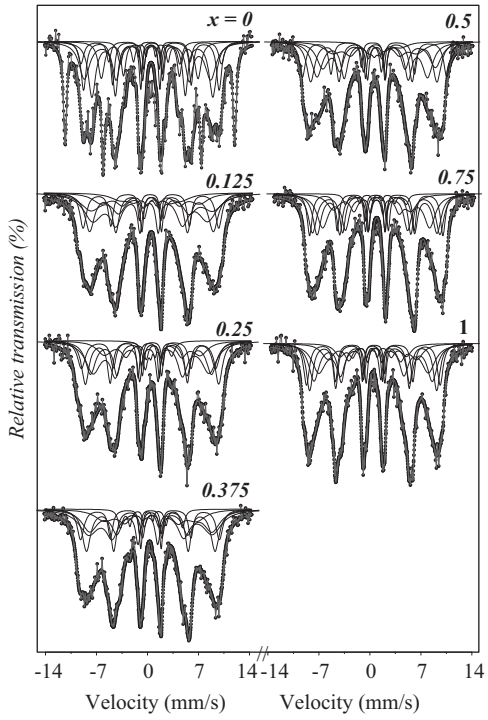

Fig. 8. Room temperature Mössbauer spectra for the system $Cd_{0.4}Mn_{0.6}Co_xFe_{2-x}O_4$.

likely to be dependent on the composition of the six A-nearest neighbors, thus the B- subpattern must be composite. Accordingly the B pattern has been fitted with multi-components B_n.

Based on the isomer shift δ, hyperfine field H, quadrupole shift ε_Q and percentage area contributed by the individual hyperfine patterns, each component has been successfully assigned to a specific configuration. The probability P of B-site Fe^{3+} ions having n A-site Cd^{2+} nearest neighbors was calculated from the binomial equation [17]:

$$P(n) = \left(\frac{6}{n}\right) f^n (1-f)^{6-n}$$

where f is the occupation percentage of Cd^{2+} ions in the A-sublattice and the Cd^{2+} ions are assumed to be distributed randomly. The calculated values are given in Table 2.

The isomer shift values of Fe^{3+} ion at the tetrahedral site δ_A and the octahedral site δ_B for the studied samples do not show dependence on x and lie in the range between 0.13 and 1.08 mm/s, where $\delta_B > \delta_A$ (Table 2). These values agree with those obtained before for spinel ferrite and are characteristic of high spin Fe^{3+} charge states [6,9,17–20]. This points to that the s-electron charge distribution of the Fe^{3+} ions in A- and B-sites is independent on the substitution process. The bond separation is smaller for A- and B-sites Fe^{3+} ions, larger overlapping of orbitals of Fe^{3+} and O^{2-} ions at A- and B-sites results in larger covalency and hence $\delta_A < \delta_B$ [8,17]. The relatively high values of δ at B_3 for x=0.125, B_3, B_4 and B_5 for x=0.25, B_3 and B_5 for x=0.5 points to the existence of Fe^{2+} ions in the sublattices [19].

The quadrupole shift ε_Q for these samples is independent on x and lies in the range 0.2 and 1.07 mm/s. The presence of relatively high values of ε_Q could be attributed to the chemical disorder in spinel structure, which produces electric field gradient (EFG) of varying magnitude, direction, sign and symmetry [8,17–20]. The relatively high values of ε_Q may be assign to the existence of Fe^{2+} ions at these sites. Siddique et al. [9], indicated that the ionic radii play a large role than their charges in the local symmetry of EFG. The quadrupole shift changes randomly with the addition x. An important contribution to EFG arises from the d-electron covalence of the Fe_B^{3+}–O^{2-} bond. As evidenced by the supertransferred hyperfine fields, the electron moves from the O^{2-} p-orbitals into the Fe_B^{3+} d-orbitals. This transfer causes a slight deformation of the spherical symmetry of the 3d electron charge density, resulting in a significant contribution to the EFG [6]. This is confirmed by the high values of the oxygen positional parameter u which are around 0.397, whereas the standard value is 0.375.

The values of the hyperfine magnetic field H at A-site (H_A) and B-sites (H_B) are given in Table 2. It is observed that the values of H_B are greater than those of H_A (except at x=0.0 and 0.125). This result is understandable in terms of the magnetic exchange interactions [17], where the magnetic moment of Co^{3+} (5.4 μ_B) is less than that of Fe^{3+} (5.92 μ_B). In most of the ferrites, the B-site hyperfine magnetic field is generally larger than that of A-site, which is attributed to the dipolar field resulting from deviation from cubic symmetry and covalent nature of tetrahedral bond [19].

Fig. 9 displays the variation of H_A and the average H_B with Co^{3+} content x. It is displayed that H_A decreases to a minimum value at x=0.25 and the trend of the average H_B increases slowly against x. This can be explained by the substitution process i.e. decreasing the number of Fe_A^{3+}–O^{2-}–Fe_B^{3+} magnetic bonds and increasing the number of Fe_A^{3+}–O^{2-}–Co_B^{3+} and to the cation distribution.

Table 2 illustrates that the line-width Γ of A-site (Γ_A) and B-site (Γ_B) changes randomly with x, which assigned to increasing the random distribution of ions among the A- and B- sublattices. The distribution of Fe ions amongst the A- and B-sites can be understood from the variation of the area ratio of B- to A- subspectra with x, as illustrated in Fig. 10. The decrease of this area ratio for $x \leq 0.25$ indicates that the number of Co^{3+} ions in the samples increases at the expense of Fe^{3+} ions at the B-sites more than those at the A-sites [9]. The increase of area ratio for $x \geq 0.375$ may reveal the introduction of Co^{3+} ions into the A-sites at this concentration.

The cation distribution of this system can be estimated using the area under the well resolved A- and B-subpatterns and the well known ionic site preferences as given in Table 3.

4. Effect of interionic distance and bond length

The dependence of the hyperfine magnetic fields H_A and H_B (average) on the bond lengths d_{AL}(Fe_A^{3+}–O^{2-}) and d_{BL}(Fe_B^{3+}–O^{2-}), respectively, is evidenced in Fig. 11. It is evidenced that H_A slightly increases versus d_{AL} for $d_{AL} \leq 2.168$ and sharply thereafter, whereas the trend of the average H_B decreases versus d_{BL}. The increase of the bond length d_{AL} reduces the d-electron covalent character of the Fe^{3+}–O^{2-} bond at these sites. This

Table 2
The obtained Mössbauer parameters for the system $Cd_{0.4}Mn_{0.6}Co_xFe_{2-x}O_4$; where H is the hyperfine magnetic field, ε_Q the quadrupole shift, δ the isomer shift, $\Gamma_{1,6}$ the line width, A_o the fractional area of each site and P the calculated probability.

x	Site	$H(T)$	QS (mm/s)	IS (mm/s)	$\Gamma_{1,6}$ (mm/s)	A_0	P
0	A	60.86	−0.26	0.30	0.44	0.17	
	B_0	50.39	0.2	0.22	0.77	0.07	0.047
	B_1	48.64	−0.07	0.37	0.71	0.14	0.187
	B_2	43.34	0.24	0.34	1.03	0.23	0.311
	B_3	42.29	−0.56	0.18	1.4	0.21	0.277
	B_4	32.37	−0.19	0.24	0.81	0.12	0.138
	B_5	21.35	−0.08	0.23	0.67	0.06	0.037
0.125	A	50	0.05	0.22	1.15	0.21	
	B_0	47.11	−0.21	0.38	0.54	0.05	0.047
	B_1	43.68	−0.09	0.7	1.42	0.13	0.187
	B_2	43.33	−0.09	0.23	1.06	0.22	0.311
	B_3	37.14	−0.01	0.25	1.64	0.24	0.277
	B_4	27.02	−0.36	0.23	1.18	0.12	0.138
	B_5	14.4	0.72	0.67	0.67	0.03	0.037
0.25	A	39.1	0.24	0.22	1.98	0.26	
	B_0	52.67	0.09	0.25	0.59	0.05	0.047
	B_1	48.45	−0.43	0.28	1.11	0.13	0.187
	B_2	48.17	0.38	0.29	1.04	0.19	0.311
	B_3	43.72	−0.11	0.41	1.44	0.2	0.277
	B_4	34.64	−0.18	0.60	2.07	0.12	0.138
	B_5	9.55	0.65	0.90	0.82	0.05	0.037
0.375	A	41.37	0.27	0.13	2.47	0.25	
	B_0	51.48	0.24	0.13	0.68	0.06	0.047
	B_1	49.82	−0.08	0.28	0.93	0.12	0.187
	B_2	46.14	−0.02	0.34	1.19	0.21	0.311
	B_3	40.94	−0.15	0.39	2.07	0.19	0.277
	B_4	33.08	−0.14	0.33	2.60	0.12	0.138
	B_5	22.33	0.41	0.20	0.64	0.05	0.037
0.5	A	40.89	−0.47	0.25	1.52	0.24	
	B_0	51.93	−0.25	0.31	0.47	0.05	0.047
	B_1	49.83	0.21	0.27	0.81	0.13	0.187
	B_2	46.73	−0.20	0.30	1.16	0.21	0.311
	B_3	41.75	0.79	0.42	1.72	0.2	0.277
	B_4	31.16	−0.04	0.32	2.44	0.12	0.138
	B_5	11.24	1.07	1.08	2.14	0.05	0.037
0.75	A	39.75	−0.05	0.25	1.63	0.24	
	B_0	52.08	0.05	0.20	0.41	0.06	0.047
	B_1	49.44	0.07	0.25	0.69	0.13	0.187
	B_2	46.20	−0.45	0.29	1.21	0.21	0.311
	B_3	45.59	0.39	0.31	1.16	0.21	0.277
	B_4	28.88	−0.52	0.23	1.74	0.12	0.138
	B_5	21.02	−0.16	0.261	0.63	0.03	0.037
1	A	40.45	0.17	0.17	1.94	0.23	
	B_0	51.58	0.10	0.18	0.36	0.04	0.047
	B_1	49.35	−0.10	0.28	0.81	0.14	0.187
	B_2	46.92	0.09	0.17	0.94	0.19	0.311
	B_3	43.69	−0.28	0.34	1.45	0.23	0.277
	B_4	32.89	−0.28	0.24	1.74	0.11	0.138
	B_5	22.98	0.125	0.18	1.33	0.07	0.037
Error		±0.2	±0.02	±0.02	±0.02	±0.01	

reduction causes the decrease in the s–d orbital overlap and hence, the hyperfine field H_A increases [9,21]. The decrease of H_B against d_{BL} may be due to the formation of clusters and diminishing of the lattice parameter a, which distort the Fe^{3+}–O^{2-} bonds. Also it may be due to the increase in the number of oxygen vacancies (i.e. growth of u) at the A-sites,

which causes an increase of the s–d orbital overlap. As a result the d-electron covalent character of the Fe^{3+}–O^{2-} bond increases, and hence H_B decreases [9,21].

The variation of H_A and the average H_B against L_A and L_B, respectively, reflects the same behavior as displayed in Fig. 12 This variation can be explained as follows; (1) the increase of L_A and L_B leads to the increase in the cation–cation overlap and s-electron density, which is reflected in increasing H_A, (2) the decrease of average H_B against L_B may be due to the fact that: the growth of the distance L_B can lead to thermal excitations at room temperature reducing the average magnetic moment of Fe^{3+}, so that the spin density transferred along the Fe^{3+}–O^{2-}–Fe^{3+} and Co^{3+}–O^{2-}–Fe^{3+} paths is diminished and (3) the formation of clusters can distort the cationic overlapping which in turn reduces H_B [9,21].

5. Conclusion

The $Cd_{0.4}Mn_{0.6}Co_xFe_{2-x}O_4$ spinel ferrite, $x=0.0$, 0.125, 0.25, 0.375, 0.5, 0.75 and 1, were prepared by the standard ceramic technique. X-ray patterns, ferromagnetic resonance (FMR) and Mössbauer spectra were used to carry out this study. X-ray patterns revealed the cubic structure of these samples. The lattice parameter, mean ionic radii and hopping and bond lengths, edges, resonance field H_r, separate energy ΔU and quality factor (Q) and the trend of the hyperfine magnetic fields, H_A and H_B, of the A- and B-sites, respectively, were decreased with the increase of Co^{3+} content x. The obtained oxygen positional parameter was higher than the standard value 0.375.

The recorded FMR and Mössbauer spectra proved the ferrimagnetic nature of all samples. The FMR spectra showed a single symmetric broad resonance signal with no sign of saturation. The line width was slightly increasing and the Lande factor (g) was increasing to a maximum value at $x=0.375$.

Mössbauer spectra were analyzed to two sextets and attributed to Fe^{3+} ions existing amongst the A- and B-sites. The subpatterns belonging to the B-site were analyzed to their multicomponents B_n. The quadrupole shift ε_Q and isomer shift δ values were found to be independent on x. The relatively high values of ε_Q and δ proved the existence of Fe^{2+} ions in

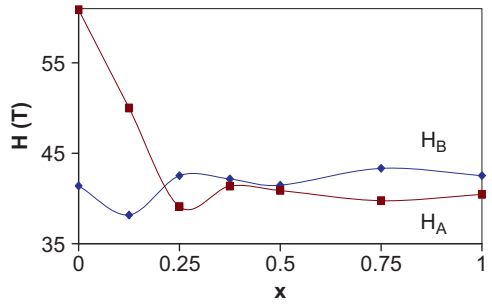

Fig. 9. The variation of the hyperfine magnetic fields, H_A and H_B, against x.

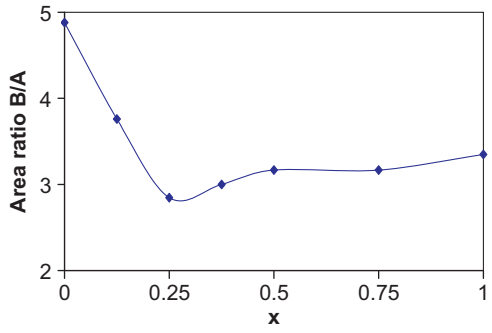

Fig. 10. The variation of area ratio of B- to A-sites with x.

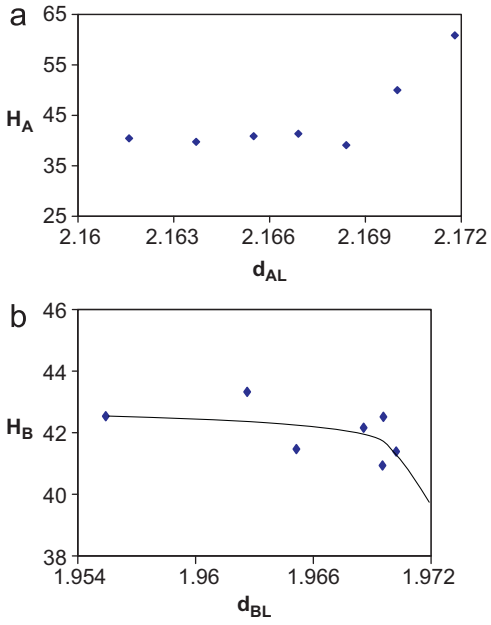

Fig. 11. The variation of (a) $H_A(T)$ versus d_{AL}(Å) and (b) average $H_B(T)$ versus d_{BL}(Å).

Table 3
The estimated cation distribution of the system $Cd_{0.4}Mn_{0.6}Co_xFe_{2-x}O_4$.

x-value	A-site	B-site
0.0	$Cd_{0.4}Mn_{0.26}Fe_{0.34}$	$Mn_{0.34}Fe_{1.66}$
0.125	$Cd_{0.4}Mn_{0.205}Fe_{0.395}$	$Mn_{0.395}Co_{0.125}Fe_{1.48}$
0.25	$Cd_{0.4}Mn_{0.145}Fe_{0.455}$	$Mn_{0.455}Co_{0.25}Fe_{1.295}$
0.375	$Cd_{0.4}Mn_{0.145}Co_{0.05}Fe_{0.405}$	$Mn_{0.455}Co_{0.325}Fe_{1.22}$
0.5	$Cd_{0.4}Mn_{0.145}Co_{0.095}Fe_{0.36}$	$Mn_{0.455}Co_{0.405}Fe_{1.14}$
0.75	$Cd_{0.4}Mn_{0.145}Co_{0.155}Fe_{0.3}$	$Mn_{0.455}Co_{0.595}Fe_{0.95}$
1	$Cd_{0.4}Mn_{0.145}Co_{0.225}Fe_{0.23}$	$Mn_{0.455}Co_{0.775}Fe_{0.77}$

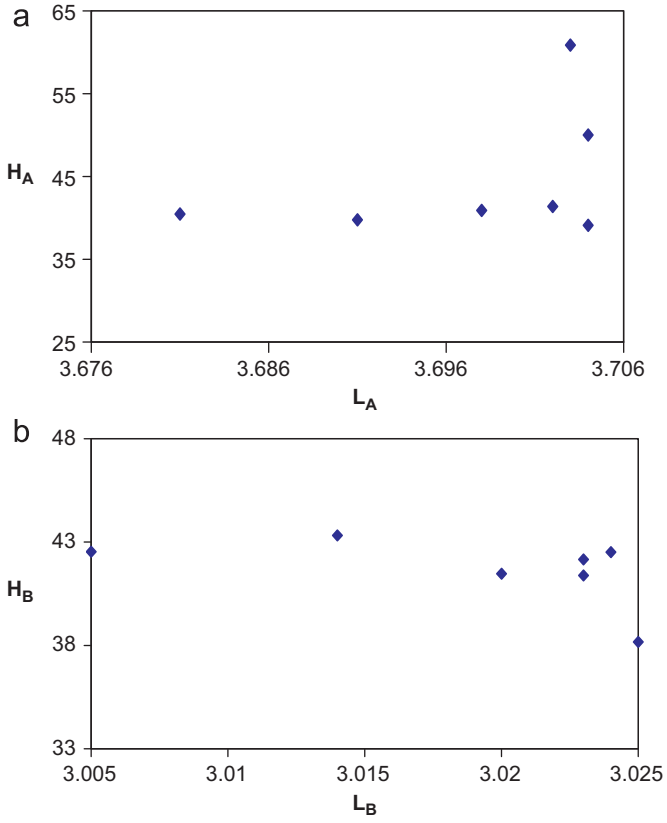

Fig. 12. The variation of (a) H_A versus L_A and (b) average H_B versus L_B.

the sample sublattices. The random change of the Mössbauer line widths Γ_A and Γ_B with x pointed to the growth of chemical disorder in the samples and presence of nonmagnetic Cd^{2+} ions at A-sites. The cation distribution of the system was estimated, where the obtained results pointed to the formation of ferrimagneticaly ordered clusters.

The hyperfine magnetic fields H_A and H_B, were affected by the hopping lengths, L_A and L_B, and bond lengths, d_{AO} and d_{BO}, at the A- and B-sites, respectively.

References

[1] A.M.M. Farea, S. Kumar, K.M. Batoo, A. Yousef, C.G. Lee, Alimuddin, Structure and electrical properties of $Co_{0.5}Cd_xFe_{2.5-x}O_4$ ferrites, Journal of Alloys and Compounds 464 (2008) 361.

[2] A.R. Shitre, V.B. Kawade, G.K. Bichile, K.M. Jadhav, X-ray diffraction and dielectric study of $Co_{1-x}Cd_xFe_{2-x}Cr_xO_4$ ferrite system, Materials Letters 56 (2002) 188.

[3] M. Maisnam, S. Phanjoubam, H.N.K. Sarma, C. Prakash, L.R. Devi, O. P. Thakur, Structural and DC resistivity behavior of Li–Mn–Ni ferrites substituted with trace amount of Co^{2+}, Physica B 370 (2005) 1–5.

[4] S. Kumar, A.M.M. Farea, K.M. Batoo, C.G. Lee, B.H. Koo, A. Yousef, Alimuddin, Mössbauer studies of $Co_{0.5}Cd_xFe_{2.5-x}O_4$ ($0.0 \le x \le 0.5$) ferrite, Physica B 1016 (2008) 1.

[5] P.K. Nayak, Synthesis and characterization of cadmium ferrite, Materials Chemistry and Physics 112 (2008) 24.

[6] M.A. Amer, Mössbauer, infrared, and X-ray studies of Ti-doped $CoCr_{1.2}Fe_{0.8}O_4$ ferrites, Physica Status Solidi A 237 (2) (2003) 459.

[7] M.A. Amer, ^{57}Fe Mössbauer, infrared and X-ray studies of the system $Zn_{1-x}Cu_xCr_{0.8}Fe_{1.2}O_4$, Physica Status Solidi 181 (2000) 539.

[8] M.A. Amer, S. Ata-Allah, T. Meaz, S. Aboul-Enein, M. Abd-El-Hamid, Mössbauer, infrared and X-ray studies for $Ni_{0.5}Zn_{0.5}Cr_xFe_{2-x}O_4$ ferrites, Turkish Journal of Physics 29 (2005) 163.

[9] M.A. Amer, Structural characterization of the $Co_{1+x}Ti_xFe_{2(1-x)}O_4$ ferrites, Physics of Low-Dimensional Structures 25/2 (2006) 96.

[10] S.S. Shinde, K.M. Jadhav, Electrical and dielectric properties of silicon substituted cobalt ferrites, Materials Letters 37 (1998) 63.

[11] JCPDS Cards no. (22-1086), (79-1155) and (73-1964), International Center for Diffraction Data, (accessed 14.10.08).

[12] S.S. Bellad, B.K. Chougule, Microstructure-dependent magnetic properties of Li–Cd ferrites, Materials Research Bulletin 8 (1998) 1165.

[13] C.T. Hsieh, J.T Lue, Anisotropy-induced quantum superparamagnet state in cobalt-ferrite nanoparticles at low temperatures, Physics Letters A 316 (2003) 329.

[14] O. Silva, P.C. Morais, Investigation of anisotropy in cadmium ferrite-based ionic magnetic fluid using magnetic resonance, Journal of Magnetism and Magnetic Materials 289 (2005) 136.

[15] N. Petchsang, W. Pon-on, J.H. Hodak and I.M. Tang, Magnetic properties of Co-ferrite-doped hydroxyl-apatite nanoparticles having a core/shell structure, Journal of Magnetism and Magnetic Materials 321, (2009), 1990.

[16] C.P. Poole, H.A. Farach, Electron spin resonance handbook, Materials Characterization, vol. 10, ASM International514.

[17] M.A. Amer, O.M. Hemeda, ^{57}Fe Mössbauer and infrared studies of the system $Co_{1-x}Cd_xFe_2O_4$, Hyperfine Interactions 96 (1995) 99.

[18] S.S. Ata-Allah, M.K. Fayek, H.S. Refai, M.F. Mostafa, Mössbauer effect study of copper containing nickel-aluminate ferrite, Journal of Solid State Chemistry 149 (2000) 434.

[19] S. Kumar, A.M.M. Farea, K.M. Batoo, C.G. Lee, B.H. Koo, A. Yousef, Alimuddin, Mössbauer studies of $Co_{0.5}Cd_xFe_{2.5-x}O_4$ ($0.0 \le x \le 0.5$) ferrite, Physica B 403 (2008) 3604.

[20] S.S. Ata-Allah, M.K. Fayek, M. Yahia, Mössbauer and DC electrical resistivity study of Zn substituted tetragonal $CuFe_{2-y}Ga_yO_4$ compound, Journal of Magnetism and Magnetic Materials 279 (2004) 411.

[21] M.A. Amer, S.A. Saafan, S.M. Attia, The effect of interionic distance on the properties of Al-doped Mn–Zn ferrites, European Physical Journal: Applied Physics 35 (2006) 201.